SPICE Simulation of Modal Impedances in Automotive Powertrains under Different Operating Conditions

Lu Wan, Abduselam Hamid, Flavia Grassi, Giordano Spadacini, Sergio A. Pignari
Dept. of Electronics, Information and Bioengineering (DEIB)
Politecnico di Milano
Milan, Italy
{lu.wan, abuduselam.hamid, flavia.grassi, giordano.spadacini, sergio.pignari}@polimi.it

***Abstract*—The spread of information-communication technology (ICT) devices in full and/or hybrid electric vehicles is posing increasing issues about coexistence between communication and electric power systems. Particularly, under different operating conditions, the time-variant and nonlinear behavior of the involved power-electronic devices may cause detrimental electromagnetic interference (EMI) effects for onboard ICT devices. The use of passive or active EMI filters can mitigate EMI, yet their effective design requires the knowledge of the actual modal impedances of the involved components. With the final objective to support EMI filter design, in this work, the frequency response of the common mode (CM) and differential mode (DM) impedances of a complete automotive power train is investigated under different operating conditions. Moreover, both low-frequency functional aspects and high-frequency parasitic effects are considered and modelled properly.**

***Index Terms*—Conducted emission, Common and differential mode, Electric vehicles.**

I. Introduction

Nowadays, full and/or hybrid electric vehicles are gaining ground in the automotive industry and among customers. Meanwhile, with the spread of ICT revolutionary applications, such as electric-control units (ECUs), global-positioning system (GPS), battery management system (BMS) and autonomous vehicles (AV), smart vehicles represent the new transportation paradigm of the future. However, switching devices, (mainly in the inverter) generate conducted emission (CE) which may give rise to coexistence issues between wired communications in ICT devices and the electric power system [1]. Once the electronic devices are disturbed, the stability of the vehicle and the safety of passengers will be affected [2].

In order to mitigate EMI using active/passive filters, both the amplitude and phase of modal impedances of the device under test (DUT) in the required frequency range should be known first [3]. Hence, several contributions were provided in recent years aimed at effective measurement of the modal impedances of switching devices, e.g., [4], [5], [6].

This project has received funding from the European Union's Horizon 2020 research and innovation programme under the Marie Skłodowska-Curie grant agreement No 812753.

Besides the amplitude and phase of modal impedance, different operating conditions should be considered in the investigation of the CEs generated by power electronics devices. In [7], a model of the converter is developed based on variable loads which significantly affect the generated DM noise. Furthermore, modal impedances could be variant under different operating conditions, which may cause lack of effectiveness if the filter is designed considering a specific working condition only. This is shown, for instance, in [8], where a novel procedure to measure the DM and CM impedance of a switched mode power supply (SMPS) under different operating conditions was presented, which makes use of an impedance analyzer (IA) and an ad hoc manufactured transformer. In general, many researchers focus directly on the measurement. However, modelling methods to investigate the DM and CM impedance of switching devices under different operating conditions need to be further investigated .

In this paper, a time-domain circuit simulation of a complete automotive powertrain with both low-frequency functional aspects and high-frequency parasitic effects is utilized to investigate the CM/DM modal impedances under different operating conditions. The rest of this paper is organized as follows. The time-domain circuit of the powertrain is described in Section II. In Section III, the proposed modelling of modal setups and the different operating conditions of the powertrain are explained. Results of CE in two conditions and modal impedances under different operating conditions are presented in Section IV. Finally, conclusions are drawn in Section V.

II. Circuit Models of Functional Units including High-frequency Effects

Fig. 1 shows the principle drawing of a typical powertrain of electric vehicles. The battery is connected to the inverter using a long dc power bus, with typical length of three to four meters. The output of the inverter is connected to the nearby three phase motor with a short ac power bus [9]. In this section, circuit models of the battery, the inverter, and the permanent-magnet synchronous motor (PMSM), representative for both low-frequency functional aspects and high-frequency parasitic effects are briefly recalled (more details can be found in [9]).

Models of ac and dc cables are here omitted for the sake of simplicity, since they do not contribute to nonlinearity in modelling modal impedances. According to [10], the presence of switching elements (e.g., IGBTs, MOSFETs, and diodes) is the main responsible for nonlinearity and time variance of the circuit.

The circuit model of the battery is inferred from [11], including specific functional parameters and high-frequency parasitic elements between phase, neutral and ground. The circuit model of the inverter is shown in Fig. 2, where the black components represent the functional parts. In the high frequency range, parasitic effects dominate the passive model of the inverter due to the internal wiring structure [12]. Therefore, all green components including R_{igbt}, L_{igbt} and C_{igbt} in parallel with the IGBTs are essential to model the behaviour of the inverter at high frequency. Regrading the model of the inverter, two specific aspects are worth to be mentioned. First, the PWM is implemented by suitable components in Simulation Program with Integrated Circuit Emphasis (SPICE). Second, IGBTs SPICE models provided by semiconductor manufactures are utilized, which can represent both the nonlinear characteristics and parasitic effects.

The circuit model of the PMSM is shown in Fig. 3. Likewise in Fig. 2, the black components (including the back-electromotive forces E_a, E_b and E_c, the winding resistance R_s and the synchronous inductance L_s) represent the classical topology of the steady-state model. The green components account for the non-ideal high-frequency behaviour. A specific topology for PMSM in electric-vehicle applications can be found in [13].

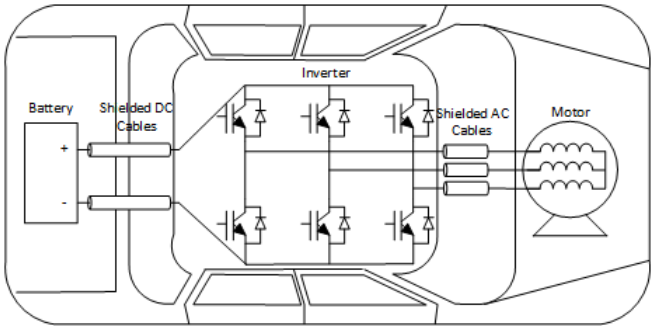

Fig. 1. General layout of the electric-vehicle powertrain.

III. Modeling of Modal Setups and Operating Conditions

A. Modeling of Modal Setups

The modal setups for simulation of DM and CM impedances are shown in Fig. 4. They are derived from [8], in which an IA and a transformer are used in the measurement setups. For SPICE simulation, the IA and transformer are replaced by the series of ideal voltage sources exciting the system at different frequencies. Particularly, for simulation of the DM impedance in Fig. 4(a), the voltage source is connected in series to an input terminal of the inverter, and the grounds of

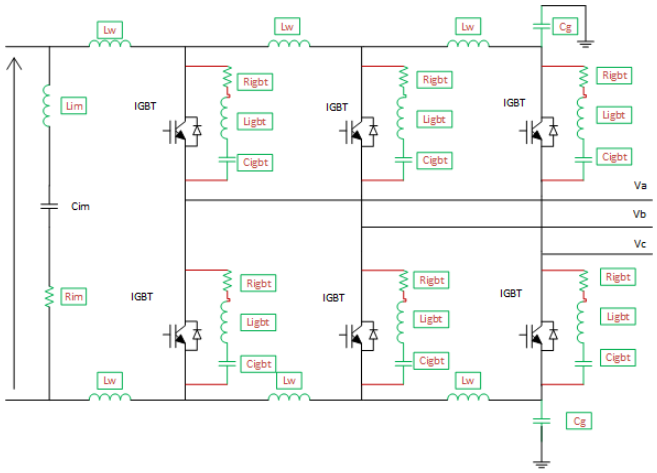

Fig. 2. Circuit model of the inverter.

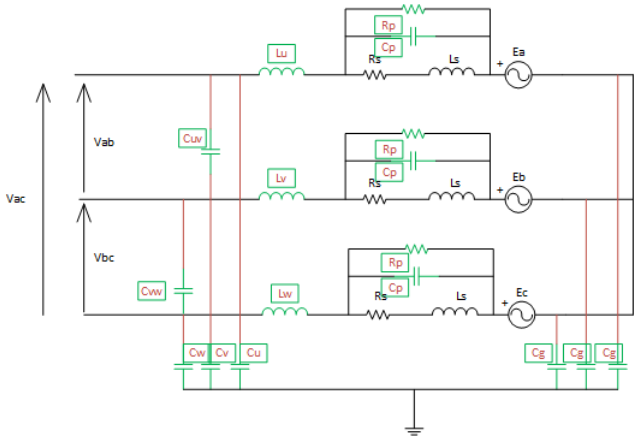

Fig. 3. Circuit model of the PMSM.

the two LISNs are connected together, so that the equivalent impedance seen between terminals L1 and L2 of the inverter and the PMSM is measured. Conversely, when simulating the CM impedance, the voltage source is included in the ground path of the system. Since the excitation provided by the voltage source is dominant, the presence of CE sources in the model are neglected. Therefore, each modal impedance is derived from two simulations: The former carried out in the absence of the DUT, the latter in the presence of the DUT.

B. Operating Conditions under Analysis

To investigate the sensitivity of CM and DM impedances to different operating conditions, the modal setups under analysis are suitably modified to reproduce different operating conditions of the system. From the features of the PMSM [13], it is possible to obtain the relationship between torque, voltage, current and the speed respectively. Based on their relationship, three different working regions are identified. In the first region (region A), the torque and current keep the nominal value, while the voltage increases proportionally with the speed till the nominal value. In the second region (region B), the voltage is constant to the nominal value, the torque decreases with

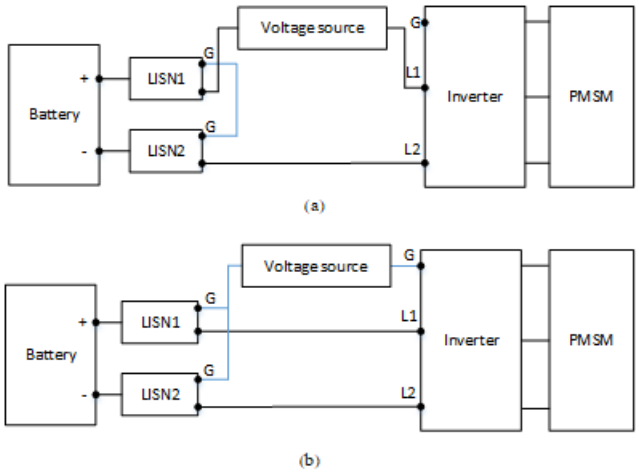

Fig. 4. Modal simulation setups.(a) DM. (b) CM.

the speed increase, and the current firstly decreases and then increases. In the third region (region C), the voltage keeps constant to the value in region B, the current takes the nominal value, and the torque continuously decreases with decreasing speed. For simulation, five operating conditions, that is points on the boundary or within the working regions of the PMSM are selected. The corresponding parameters are collected in the Tab. I, where: P_m is the mechanical power, T_e is the torque, V_{rms} is the root mean square (RMS) value of the input voltage, I_{rms} is the RMS value of the input current, n_m is the speed of the rotor, f is the operating frequency of the motor, and E_{rms} the back-electromotive force. Point P_A and P_C are selected in region A and C, respectively. Three points are selected in region B. Namely, P_B and P are at the boundaries of region B, meanwhile, P_N is associated with nominal working condition. The above mentioned parameters should be modified in the simulation model of the PMSM, according to different conditions. Also, the frequency of the control signal in the PWM of the inverter should be modified, so to be consistent with f. Conversely, the circuit models of the battery and LISN remain the same in every operating condition. In addition to the aforesaid operating conditions, the condition in which the system is switched off is also considered, and realized by short-circuiting the dc voltage in the battery, the PWM sources of the inverter and the back-electromotive forces in the PMSM.

TABLE I
OPERATING CONDITIONS UNDER ANALYSIS

	P_A	P_N	P_B	P	P_C
P_m(kW)	25	50	50	50	30
T_e(Nm)	136.4	136.4	119.4	101.8	53
V_{rms}(V)	61	122	122	122	122
I_{rms}(I)	147	147	135	147	147
n_m(rpm)	1750	3500	4000	4630	5417.5
f(Hz)	58.5	117	133.3	156.3	180.5
E_{rms}(V)	57	114	130	153	176.5

IV. SIMULATION OF CES AND MODAL IMPEDANCES

A. Simulation of DM and CM noise voltages

In this subsection, the CEs generated under the five operating conditions in Tab. I were investigated. The CM and DM noise voltages simulated for point P_A and P_C are compared in Fig. 5 and Fig. 6, respectively. For both conditions, CM noise voltages are almost overlapping in the frequency interval from 10 kHz to 30 MHz with small differences variation in amplitude at specific frequency components only. Particularly, at low frequency, i.e., up to nearly 300 kHz, CM emissions look smaller for point P_C, yet at high frequency the comparison is reversed. Apart from these differences, it can be concluded that CM CEs are not significantly affected by the specific operating conditions under analysis.

The corresponding DM noise voltages are compared in Fig. 6, which puts in evidence a prevalence of the emissions generated for the working condition identified by point P_C also in the intermediate frequency range from 1 MHz to nearly 10 MHz.

A part from the specific working conditions, which do not seem to significantly impact on the generated CEs, the comparison between the CE spectra plotted in the two figures put in evidence the prevalence of CM CEs nearly in the whole frequency interval under investigation.

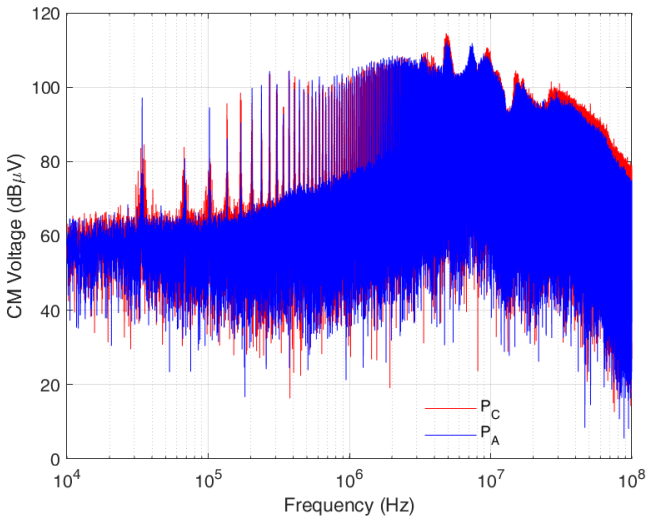

Fig. 5. CM noise voltages for the operating conditions identified by points P_A (blue spectrum) and P_C (red spectrum).

B. Simulation of the CM Impedance

In order to investigate the frequency response of the CM impedance in the interval from 10 kHz to 30 MHz, twelve sinusoidal voltage sources (with frequency 10 kHz, 20 kHz, 40 kHz, 50 kHz, 80 kHz, 100 kHz, 500 kHz 1 MHz, 5 MHz, 10 MHz, 20 MHz and 30 MHz) in series were used to realize the voltage source in Fig. 4(b). For the six operating conditions under analysis (i.e., those in Tab. I and the switching-off mode), time-domain circuit simulations were carried out in SPICE,

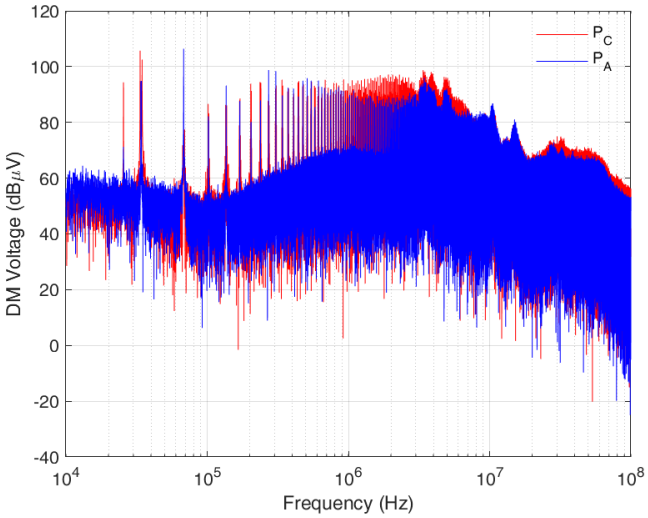

Fig. 6. DM noise voltages for the operating conditions identified by points P_A (blue spectrum) and P_C (red spectrum).

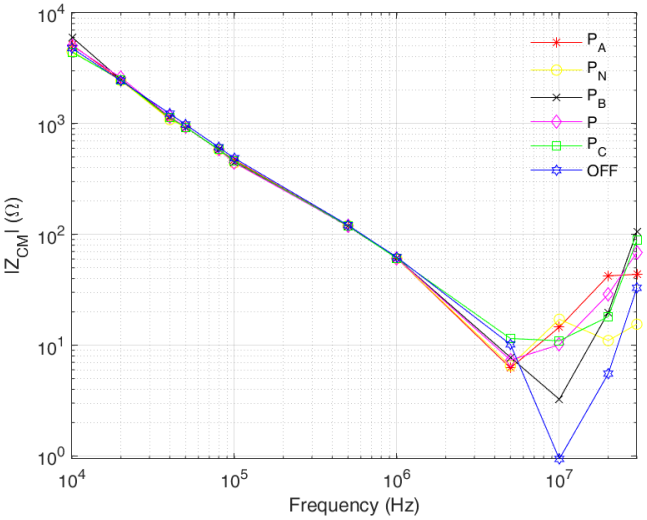

Fig. 7. Frequency response of the amplitude of CM impedance under different operating conditions.

and the frequency response of the CM impedance (amplitude and phase) was afterwards derived using interpolation and Fast Fourier Transform (FFT).

The frequency response of both amplitude and phase of CM impedance is plotted in Fig. 7 and Fig. 8, respectively. From the frequency response of the phase, it is quite clear that all CM impedances in every operating condition exhibit a capacitive behaviour up to 1 MHz. For all operating conditions, the obtained CM impedances are almost the same (including the switching-off mode), although some deviations found beyond 1 MHz, which may be due to the resonances of the whole system. One can conclude that the CM impedance is mainly dominated by the parasitic coupling capacitors in the system, as previously observed by measurements, e.g., in [8].

C. Simulation of DM Impedance

For investigating the frequency behavior of the DM impedance, the aforesaid set of simulations was carried out, considering the modal test setup in Fig. 4(a). For the working conditions under analysis, the obtained frequency responses of the amplitude and phase of the DM impedance are compared in Fig. 9 and Fig. 10, respectively. With the only exception of the switching-off condition, the amplitude of the impedances obtained for all the other operating conditions is similar. Moreover, the corresponding phase plot reveals that for all the five operating conditions under study the DM impedance exhibits an inductive behaviour, except for some resonance frequencies around 20 kHz.

However, for the switching-off condition both the amplitude and phase of the DM impedance show quite different patterns with respect to other conditions. More specifically, the phase plot shows that the DM impedance in the switching-off condition is dominated by parasitics below 80 kHz and above 1 MHz. The impedance amplitude below 1 MHz is quite small. In general, one can conclude that the DM impedance is

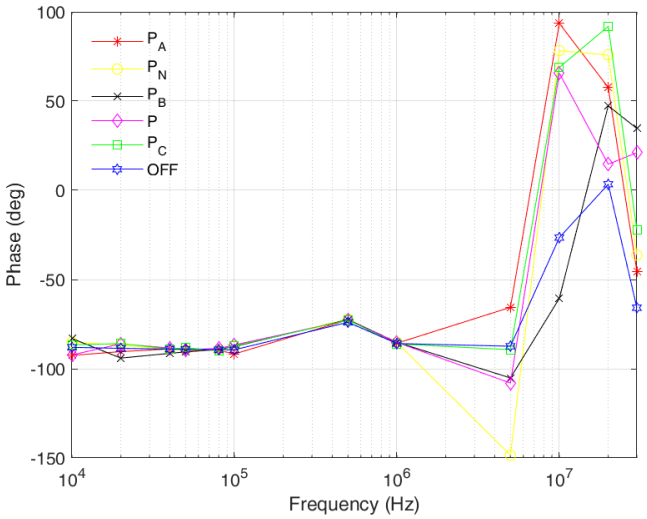

Fig. 8. Frequency response of the phase of CM impedance under different operating conditions.

basically inductive and is less correlated to parasitic elements. From the comparison with the switching-off condition, the DM impedance could have a stronger relationship with the input DC voltage and the load than with parasitic elements.

V. Conclusion

In this work, the frequency response of the amplitude and phase of the CM and DM impedances of an automotive powertrain was investigated by simulations under different operating conditions, with the final objective to support the design of suitable EMI filters to reduce the CE generated by the inverter and propagating along the power cables. The presented circuit model includes both low-frequency functional

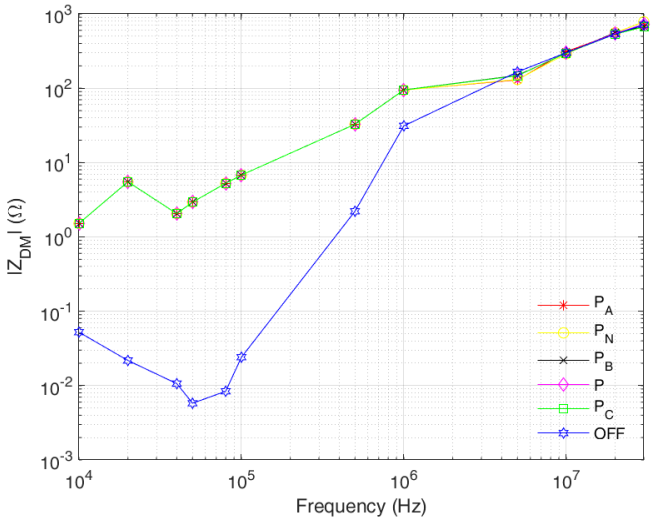

Fig. 9. Frequency response of the amplitude of DM impedance under different operating conditions.

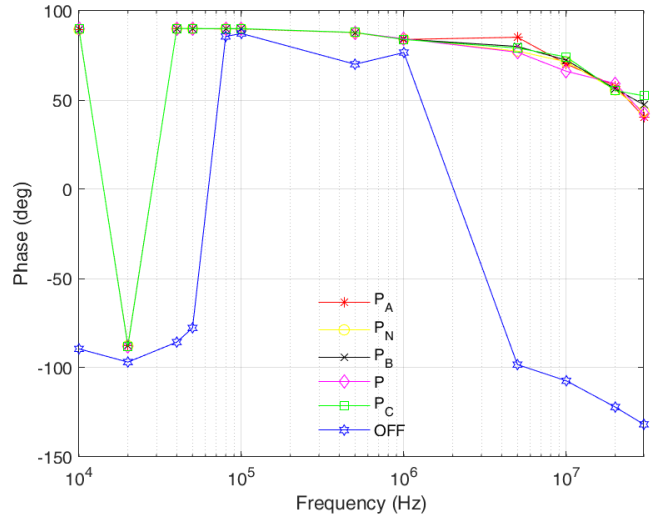

Fig. 10. Frequency response of the phase of DM impedance under different operating conditions.

aspects and high-frequency parasitic effects and allows time-domain simulations.

It was observed that the CM impedance mainly depends on the parasitic capacitive coupling path, that is, it is basically independent from the specific operating condition of the powertrain. Instead, the frequency response of the DM impedance of the converter switched-on resulted to be significantly different from the one simulated in the switching-off mode. The observed sensitivity of the DM impedance to the operating conditions needs to be taken into due consideration for effective design of the EMI filter. Particularly, the proposed simulation results suggest that such an impedance should be measured with the converter switched on and in different operating conditions, in order to provide exhaustive information for effective design and estimation of filter performance. These conclusions are in line with the experimental results shown in [8], which were obtained from measurements carried out on a different converter, by considering different operating conditions.

References

[1] F. Grassi and S. A. Pignari, "Immunity to conducted noise of data transmission along dc power lines involving twisted-wire pairs above ground," *IEEE Transactions on Electromagnetic Compatibility*, vol. 55, no. 1, pp. 195–207, 2012.

[2] Y. Guo, L. Wang, and C. Liao, "Modeling and analysis of conducted electromagnetic interference in electric vehicle power supply system," *Progress In Electromagnetics Research*, vol. 139, pp. 193–209, 2013.

[3] V. Tarateeraseth, K. Y. See, F. G. Canavero, and R. W.-Y. Chang, "Systematic electromagnetic interference filter design based on information from in-circuit impedance measurements," *IEEE Transactions on Electromagnetic Compatibility*, vol. 52, no. 3, pp. 588–598, 2010.

[4] D. Zhang, D. Y. Chen, M. J. Nave, and D. Sable, "Measurement of noise source impedance of off-line converters," *IEEE Transactions on Power Electronics*, vol. 15, no. 5, pp. 820–825, 2000.

[5] F. Zheng, W. Wang, X. Zhao, M. Cui, Q. Zhang, and G. He, "Identifying electromagnetic noise-source impedance using hybrid of measurement and calculation method," *IEEE Transactions on Power Electronics*, vol. 34, no. 10, pp. 9609–9618, 2019.

[6] V. Tarateeraseth, B. Hu, K. Y. See, and F. G. Canavero, "Accurate extraction of noise source impedance of an smps under operating conditions," *IEEE Transactions on Power Electronics*, vol. 25, no. 1, pp. 111–117, 2009.

[7] Q. Liu, F. Wang, and D. Boroyevich, "Model conducted emi emission of switching modules for converter system emi characterization and prediction," in *Conference Record of the 2004 IEEE Industry Applications Conference, 2004. 39th IAS Annual Meeting.*, vol. 3. IEEE, 2004, pp. 1817–1823.

[8] E. Mazzola, F. Grassi, and A. Amaducci, "Novel measurement procedure for switched-mode power supply modal impedances," *IEEE Transactions on Electromagnetic Compatibility*, 2019.

[9] G. Spadacini, F. Grassi, and S. A. Pignari, "Modelling and simulation of conducted emissions in the powertrain of electric vehicles," *Progress In Electromagnetics Research*, vol. 69, pp. 1–15, 2016.

[10] S. Banerjee and G. C. Verghese, *Nonlinear phenomena in power electronics*. IEEE, 1999.

[11] M. Reuter, S. Tenbohlen, and W. Köhler, "The influence of network impedance on conducted disturbances within the high-voltage traction harness of electric vehicles," *IEEE Transactions on Electromagnetic Compatibility*, vol. 56, no. 1, pp. 35–43, 2013.

[12] M. Reuter, T. Friedl, S. Tenbohlen, and W. Köhler, "Emulation of conducted emissions of an automotive inverter for filter development in hv networks," in *2013 IEEE International Symposium on Electromagnetic Compatibility*. IEEE, 2013, pp. 236–241.

[13] R. Staunton, S. Nelson, P. Otaduy, J. McKeever, J. Bailey, S. Das, and R. Smith, *PM motor parametric design analyses for a hybrid electric vehicle traction drive application*. United States. Department of Energy, 2004.